Structure, Vol. 10, 1637–1648, December, 2002, ©2002 Elsevier Science Ltd. All rights reserved. PII S0969-2126(02)00904-8

Structure of the Monomeric Isocitrate Dehydrogenase: Evidence of a Protein Monomerization by a Domain Duplication

Yoshiaki Yasutake,[2] Seiya Watanabe,[2] Min Yao, Yasuhiro Takada, Noriyuki Fukunaga, and Isao Tanaka[1]
Division of Biological Sciences
Graduate School of Science
Hokkaido University
Kita-10, Nishi-8
Kita-ku, Sapporo, Hokkaido 060-0810
Japan

Summary

NADP$^+$-dependent isocitrate dehydrogenase is a member of the β-decarboxylating dehydrogenase family and catalyzes the oxidative decarboxylation reaction from 2*R*,3*S*-isocitrate to yield 2-oxoglutarate and CO_2 in the Krebs cycle. Although most prokaryotic NADP$^+$-dependent isocitrate dehydrogenases (IDHs) are homodimeric enzymes, the monomeric IDH with a molecular weight of 80–100 kDa has been found in a few species of bacteria. The 1.95 Å crystal structure of the monomeric IDH revealed that it consists of two distinct domains, and its folding topology is related to the dimeric IDH. The structure of the large domain repeats a motif observed in the dimeric IDH. Such a fusional structure by domain duplication enables a single polypeptide chain to form a structure at the catalytic site that is homologous to the dimeric IDH, the catalytic site of which is located at the interface of two identical subunits.

Introduction

The β-decarboxylating dehydrogenases catalyze the Mg^{2+}- and NAD(P)$^+$-dependent hydride transfer at C2 and then the Mg^{2+}-dependent decarboxylation at C3 of (2*R*,3*S*)-2-hydroxy acids. This protein family involves three members, NADP$^+$-dependent isocitrate dehydrogenase (EC 1.1.1.42; NADP$^+$-IDH), NAD$^+$-dependent isocitrate dehydrogenase (EC 1.1.1.41; NAD$^+$-IDH), and NAD$^+$-dependent isopropylmalate dehydrogenase (EC 1.1.1.85; NAD$^+$-IPMDH). IDH catalyzes the oxidative decarboxylation reaction of 2*R*,3*S*-isocitrate to yield 2-oxoglutarate and CO_2 in the Krebs cycle [1]. The 2-oxoglutarate is known to be a key substance in biosyntheses of cell constituents via reductive amination to glutamate. NAD$^+$-IDHs, which form the heterooligomeric structure, are found only in the eukaryotic organisms, while NADP$^+$-IDHs, which form the dimeric structure composed of identical subunits of 40–50 kDa, are found in a wide variety of both prokaryotic and eukaryotic organisms [1]. NAD$^+$-IPMDH, another homodimeric molecule, catalyzes the oxidative decarboxylation reaction of 3-isopropylmalate to yield 2-oxoisocaproate and CO_2. Crystal structures of the homodimeric IDH and IPMDH revealed that these two enzymes are structurally homologous and are unique in their lack of the Rossmann fold, a common nucleotide binding motif [2, 3].

In contrast to these homologous proteins, NADP$^+$-dependent monomeric IDHs with molecular weights of 80–100 kDa are found in a few species of bacteria, i.e., *Azotobacter vinelandii* [4], *Colwellia maris* [5], *Corynebacterium glutamicum* [6], *Rhodomicrobium vannielii* [7], *Vibrio parahaemolyticus* [8], and *Desulfobacter vibrioformis* [9]. The genes encoding the monomeric IDH have already been cloned and sequenced from *A. vinelandii* [10], *C. maris* [11], and *C. glutamicum* [6]. In addition, recent genome projects have revealed several putative genes encoding the monomeric IDH in extra bacteria, i.e., *Campylobacter jejuni* (National Center for Biotechnology Information [NCBI] database accession number NP_281715), *Mycobacterium leprae* (NP_302705), *Mycobacterium tuberculosis* (NP_214580), *Neisseria meningitides* (NP_273960), *Pseudomonas aeruginosa* (NP_251314), *Streptomyces coelicolor* (CAB88977), *Vibrio cholerae* (NP_230786), and *Xylella fastidiosa* (NP_299977). Although the sequence alignment within monomeric IDHs from *A. vinelandii*, *C. maris*, and *C. glutamicum* shows almost 50%–60% complete similarity, no homology has been found between the monomeric and dimeric IDHs [10].

Monomeric IDHs seem to play crucial roles in these bacteria. The nitrogen-fixing bacterium *Azotobacter vinelandii* possesses the monomeric IDH abundantly in the cytoplasm. The high concentration of this enzyme, which accounts for 1%–2% of the total soluble protein of the organism, suggests that it plays an important role in energy production and nitrogen fixation [4]. *A. vinelandii* IDH shows an exceptionally high v_{max} value, and it reduced 722 μmol of NADP$^+$ per minute per milligram of protein at 37°C [12]. An obligately psychrophilic marine bacterium, *Colwellia maris*, is also unique in that it possesses both monomeric and dimeric IDHs. Transcription of the *icdI* and *icdII* genes, which encode the dimeric IDH (IDH-I) and the monomeric IDH (IDH-II), respectively, is regulated in response to environmental factors. The *icdII* gene was found to be a low-temperature-inducible gene, and the IDH-II consequently presents a cold adaptation; K_m values of IDH-II for isocitrate and NADP$^+$ at 4°C are 25-fold and 70-fold larger, respectively, than those of IDH-I. Furthermore, IDH-II is completely inactivated above 20°C, as shown in both in vitro and in vivo experiments [13]. These results suggest that IDH-II is indispensable for the survival of this bacterium in a low-temperature environment. The cold adaptation of this enzyme has been shown to enable a transformed *E. coli* mutant to grow at low temperature [13].

The monomeric IDH unambiguously catalyzes a reaction identical to that of the dimeric IDH using the single polypeptide chain. Since the catalytic site of the dimeric

[1]Correspondence: tanaka@castor.sci.hokudai.ac.jp
[2]These authors contributed equally to this work.

Key words: crystal structure; gene duplication; 3D domain swapping; monomeric IDH; molecular evolution; β-decarboxylating dehydrogenase family

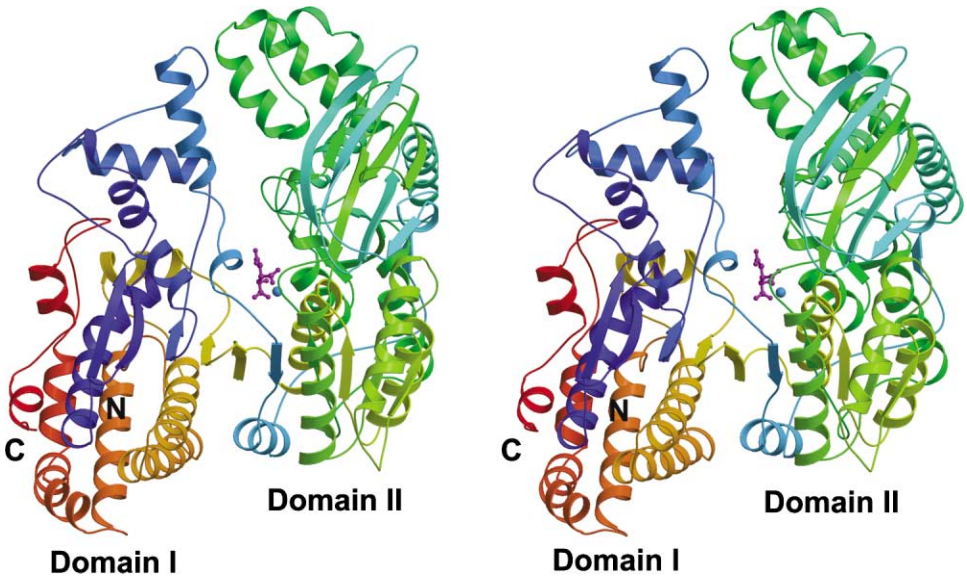

Figure 1. Stereo View Ribbon Diagram of the Monomeric IDH Complexed with Isocitrate and Mn^{2+}

The molecule consists of two distinct domains, a small domain (domain I) and a large domain (domain II). The isocitrate and Mn^{2+} binding site is located at the interface between these two domains. The ribbon model is colored according to sequence by a rainbow color ramp from blue at the N terminus to red at the C terminus. The isocitrate molecule is represented as a ball and stick model (magenta), and Mn^{2+} is represented as a ball model (blue).

IDH is located at the interface of two identical subunits and is composed of the residues from both subunits [2], it is of considerable interest in terms of the structure of the catalytic site of the monomeric IDH. The studies of the immunological crossreactivity suggest that these two IDHs are not structurally homologous [7, 8], and it has been considered that the monomeric and dimeric IDHs have convergently evolved independently from the different ancestral genes. Very recently, however, Chen and Yang performed a partial sequence alignment of the monomeric IDH from *C. glutamicum* with the sequences of dimeric IDHs and found that a few fragments, including several putative catalytic residues, were common to both the monomeric and dimeric IDHs [14]. These findings were in remarkable contrast to those of an immunological study, and, thus, no conclusive evidence about the evolutional relationship between these two IDHs has yet been reported.

One of the best ways to understand the structural and evolutional relationship between the monomeric and dimeric IDHs is to determine the three-dimensional structure of the monomeric IDH by a crystallographic approach. The first preliminary crystallographic study of the *A. vinelandii* IDH was made more than 20 years ago [15]. Nevertheless, crystal structure analysis of the monomeric IDH has not been achieved until the present study. We successfully purified and crystallized the monomeric IDH from the nitrogen-fixing bacterium *Azotobacter vinelandii*, in the presence of isocitrate and Mn^{2+}. Because the crystals of the *A. vinelandii* IDH were too fragile to soak in a heavy-atom solution for the preparation of heavy-atom-substituted crystals, we applied the Mn atom as an anomalous scatterer for the multiwavelength anomalous diffraction (MAD) method. This is the first trial to perform the protein structure analysis with only the Mn atom as an anomalous scatterer [16]. In the present paper, we describe the 1.95 Å crystal structure of the monomeric IDH from *A. vinelandii* complexed with isocitrate and Mn^{2+}. The structure revealed not only the critical amino-acid residues for isocitrate and Mn^{2+} binding, but also the reason why the single polypeptide chain is able to catalyze a reaction identical to that of the dimeric IDH. Furthermore, the folding topology undeniably contains clues as to whether these IDHs originated from a shared ancestral gene or evolved convergently.

Results and Discussion

Overall Structure

The crystal structure of the monomeric IDH from *Azotobacter vinelandii* complexed with isocitrate and Mn^{2+} was determined to a resolution of 1.95 Å by the MAD method. Only one manganese atom per monomeric IDH molecule with a molecular weight of 80 kDa was present and was used as an anomalous scatterer for the MAD phase calculation (see Experimental Procedures). The refined structural model of the monomeric IDH revealed that the molecule consists of two distinct domains with different sizes (Figures 1 and 2A). The small domain (domain I), which contains both the N- and C-terminal segments, is composed of five β strands (β1–β5) and 14 α helices (α1–α6 and α20–α27). The peripheral helix-rich region of domain I, located near the C-terminal segment, consists of eight α helices (α1 and α21–α27). The four-helix bundle motif composed of α1 and α21–α23 is also located in this region. The other conformation of domain I generally falls into an α plus β classification. The large domain (domain II) is composed of 16 β strands (β6–β21) and 13 α helices (α7–19). In domain II,

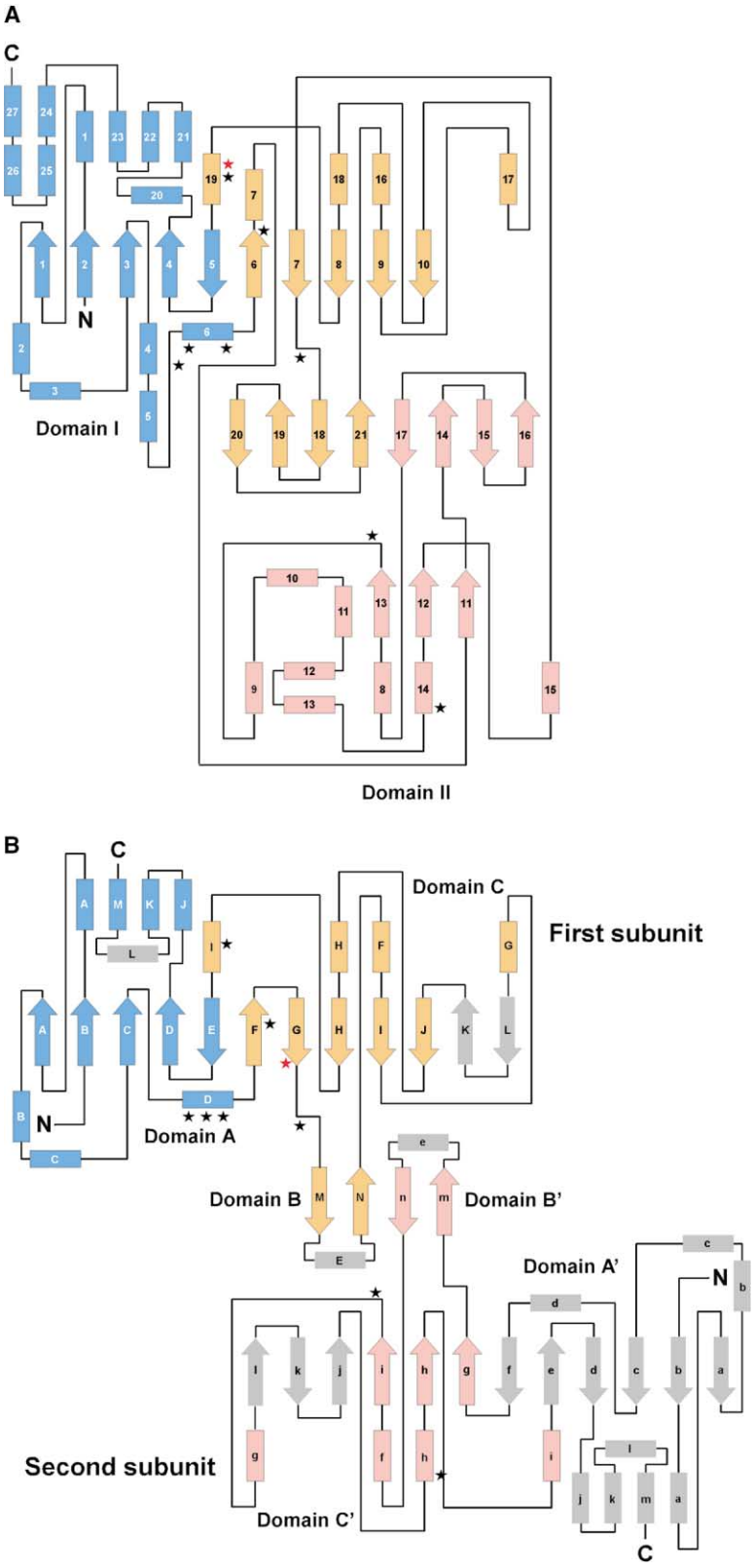

Figure 2. Topological Comparison between the Monomeric and Dimeric IDH

The stars represent substrate and metal ion binding residues. The red stars represent the arginine residues that are functionally related, but not conserved in a sequence level (see text).

(A) The topological diagram of the monomeric IDH from *A. vinelandii*. The blue structure corresponds to domain I, and the orange and pink structure corresponds to domain II, consisting of two repetitive motifs. The orange structure is related to the pink structure by a pseudo-2-fold axis. The region consisting of β14–β21 corresponds to the unique arm-like conformation, which consists of two symmetrically arranged Greek key motifs.

(B) The topological diagram of the homodimeric IDH from *E. coli* [2]. This figure schematically shows both identical subunits related by a crystallographic 2-fold axis, for comparison with the folding topology of the monomeric IDH in diagram (A). The blue structure corresponds to domain A, the orange structure corresponds to domain B-C of the first subunit, and the pink structure corresponds to domain B-C of the second subunit. In this diagram, the segments in gray are not present in the monomeric IDH. The region consisting of βM (m), βN (n), and αE (e) forms a clasp-like domain (domain B).

3 of the 16 β strands (β11–β13) form the three-stranded parallel β sheet, and 8 of the 16 β strands (β14–β21) form a unique arm-like conformation that protrudes from domain II. This arm-like conformation is formed by a symmetrical arrangement of two Greek key motifs (β14–β17 and β18–β21). The other topology in domain II gen-

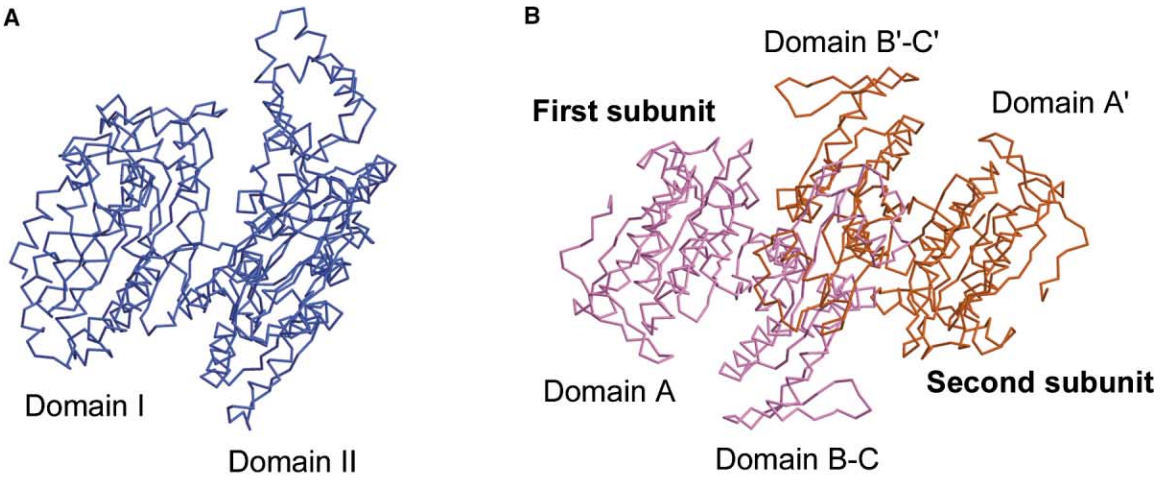
A
Domain I
Domain II
B
Domain B'-C'
First subunit
Domain A'
Domain A
Second subunit
Domain B-C

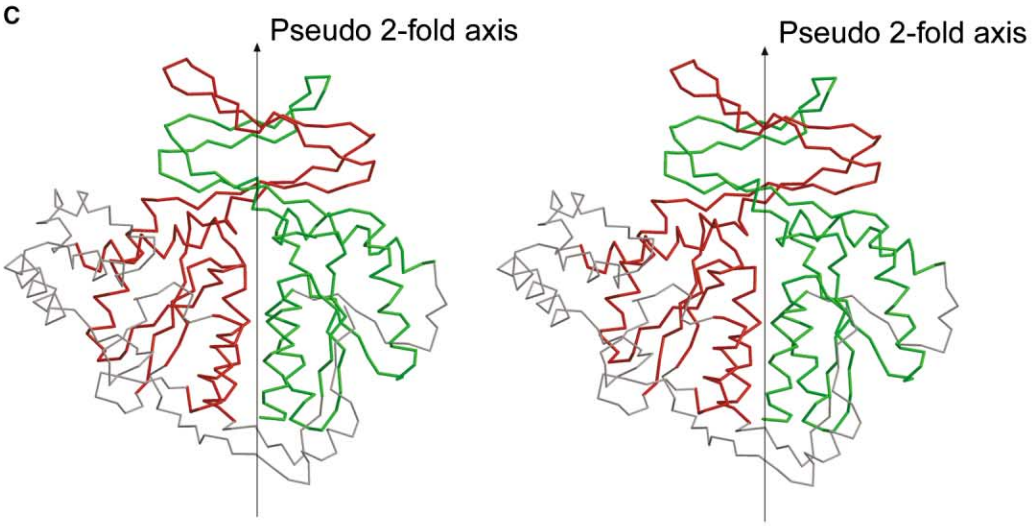
C
Pseudo 2-fold axis
Pseudo 2-fold axis

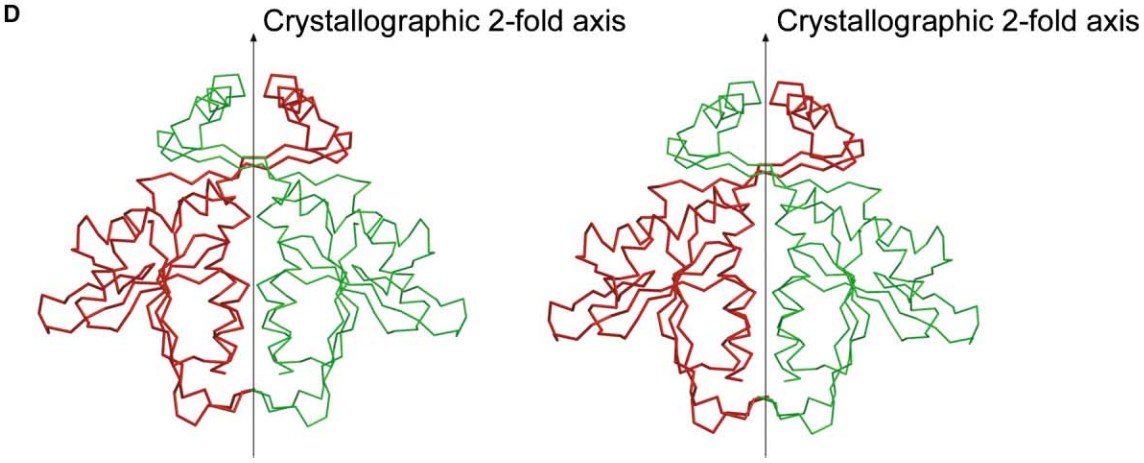
D
Crystallographic 2-fold axis
Crystallographic 2-fold axis

erally falls into an α/β or α plus β classification. The central sheet region that spans both domains I and II forms an open twisted β sheet motif composed of eight parallel (β1–β4 and β7–β10) and two antiparallel β strands (β5–β6). The substrate and Mn^{2+} binding site is located at the bottom of the hydrophilic cleft between these two domains.

Structural Relationship with the Dimeric IDH

We compared the structure of the monomeric IDH from *Azotobacter vinelandii* with that of the *Escherichia coli* IDH [2], which is one of the best characterized of the dimeric IDHs that are composed of two identical subunits. The dimeric IDH is divided into three distinct domains: a large domain (domain A) (βA–βE, αA–αD, and αJ–αM), a clasp-like domain (domain B) (βM–βN and αE), and a small domain (domain C) (βF–βL and αF–αI) [2]. The topological diagrams of the monomeric and dimeric IDHs are shown in Figure 2. Although the amino acid sequences of the monomeric and dimeric IDHs are quite different from one another [10], the folding topology of the monomeric IDH is related to that of dimeric IDH. A DALI structural similarity search [17] also revealed that the structure of the monomeric IDH is significantly similar to those of the dimeric IDH [18] (Protein Data Bank ID 1ISO; Z score, 15.9; rms deviation, 3.7 Å for 342 Cα atoms) and IPMDH [19] (Protein Data Bank ID 1CNZ-A; Z score, 18.1; rms deviation, 3.2 Å for 342 Cα atoms).

The monomeric IDH is created by fusing the partial structures of the two subunits of the dimeric IDH with substantial mutations; it consists of all three domains from the first subunit and domains B and C from the second subunit of the dimeric IDH (Figure 2). The single polypeptide chain of the monomeric IDH, in practice, is arranged between the N and C termini in the order of N-terminal domain A (first subunit), domain B (second subunit), domain C (second subunit), domain B (first subunit), domain C (first subunit), and C-terminal domain A (first subunit). Domain I of the monomeric IDH corresponds to domain A, and domain II of the monomeric IDH consists of the repetitive motif composed of the domains B and C from both subunits. The repetitive domain B in domain II corresponds to a unique arm-like conformation with double Greek key motifs, substituting one α helix (αE or αe) of the dimeric IDH with two β strands (β15–β16 or β19–β20). Crystal structure analysis of the dimeric IDH has shown that two identical subunits are related by a crystallographic 2-fold axis (Figures 3B and 3D) [2, 20]. A similar pseudo-2-fold axis exists only in domain II of the monomeric IDH (Figures 3A and 3C). Indeed domain II cannot be separated into two equivalent regions, precisely because of the insertions, such as that of four α helices (α10–α13). Such a fusional structure suggests that the monomeric IDH originated from the partial duplication of the shared ancestral gene, rather than the convergent evolution from different genes.

In contrast to the conservation of tertiary structures between the monomeric and dimeric IDHs, the homology of the amino acid sequences is no more than 7%–8%. Figure 4A shows the structure-based sequence alignment of the monomeric and dimeric IDHs. Although some conserved residues, including most of the substrate and metal ion binding residues (with the exception of Arg547; see next section), are found by the structure-based sequence alignment, many residues cannot be aligned at all, especially in most loop regions. These remarkable differences in the amino acid residues and chain lengths suggest that the monomeric IDH molecule has experienced the cumulative insertion and deletion events during molecular evolution.

Substrate and Mn^{2+} Binding Residues

Both the monomeric and dimeric IDHs have the same coenzyme specificity, require divalent metal cations for maximum activation, and catalyze the identical reaction. In light of these biochemical similarities, the structure of the monomeric IDH is of great interest, particularly at the catalytic site. The catalytic site of the dimeric IDH is located at the interface of two identical subunits and formed with the side chains of the amino acid residues derived from both subunits [2, 20]. The crystal structure of the monomeric IDH reveals that the single polypeptide chain has acquired the ability to catalyze a reaction identical to that of the dimeric IDH by fusing domains B and C of the second subunit while maintaining their spatial relationship (Figure 5). All of the substrate and metal cation binding residues are clearly defined in the structure of the monomeric IDH. Hydrogen bonds are formed between isocitrate and Ser132, Asn135, Arg139, Arg145, Arg547, Tyr420, and Lys255 of the monomeric IDH, corresponding to Ser113, Asn115, Arg119, Arg129, Arg153, Tyr160, and Lys230′ of the *E. coli* IDH, respectively (the prime sign indicates the second subunit). The

Figure 3. Cα Trace of the Monomeric and Dimeric IDHs Showing the Similarities in the Structures

(A) Cα trace of the monomeric *A. vinelandii* IDH. The folding of the single polypeptide chain of the monomeric IDH creates a fusional structure. Domain II consists of domain B-C of the first subunit and that of the second subunit of the dimeric IDH. The pseudo-2-fold axis, which coincides with the crystallographic 2-fold axis shown in (B), is located at the center of domain II. This symmetry relates two repetitive structural motifs in domain II, as shown in (C).

(B) Cα trace of the homodimeric form of the *E. coli* IDH. Two identical subunits are colored in magenta (the first subunit) and in orange (the second subunit), respectively. The crystallographic 2-fold axis is present in the center of the homodimeric form of the *E. coli* IDH and relates these two identical subunits.

(C) Stereo view Cα trace of the overall domain II of the monomeric IDH. Domain II consists of two structurally homologous motifs (β11-β14-β15-β16-β17-α8-β13-α9-α14-β12-α15, red; β7-β18-β19-β20-β21-α16-β9-α17-α18-β8-α19, green), corresponding to domains B-C and B′-C′ of the dimeric IDH. These structural motifs are related by the pseudo-2-fold axis shown in this figure. Regions that are not structurally conserved with each other (mainly α10–α13) are colored in gray. One of the homologous motifs can be superimposed onto another by rotating on the pseudo-2-fold axis with an rms deviation of 3.5 Å on the 146 Cα atoms colored in red or green.

(D) Stereo view Cα trace of two B-C domains of the dimeric *E. coli* IDH. The two B-C domains (red and green, respectively) are related by the crystallographic 2-fold axis.

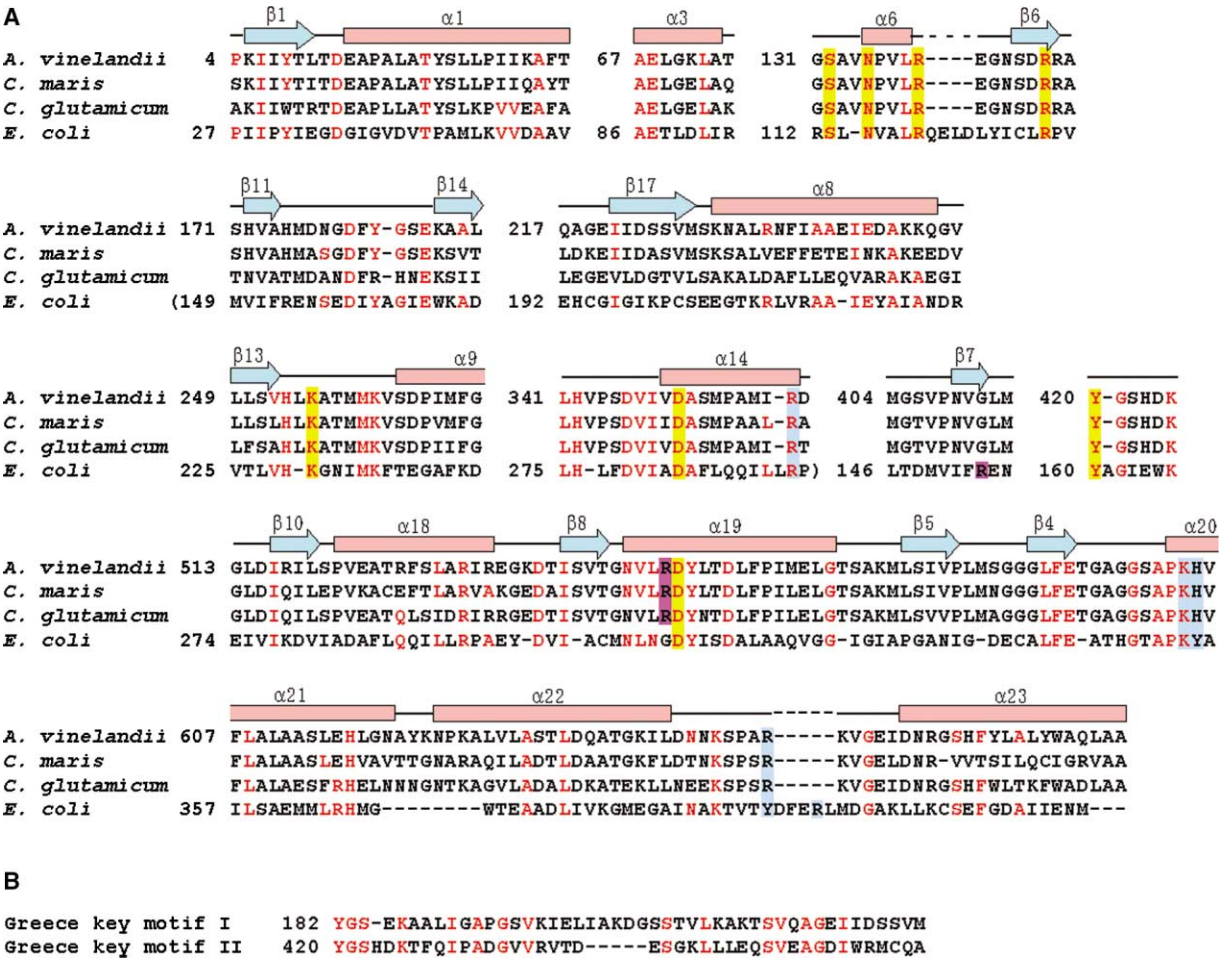

Figure 4. Sequence Alignment

(A) The structure-based sequence alignment between the monomeric IDHs from *A. vinelandii*, *C. maris*, and *C. gulutamicum* and dimeric IDH from *E. coli*. In this figure, 301 out of 741 residues, which can both structurally and sequentially be related between the monomeric and dimeric IDHs, are shown. Sequences in parentheses correspond to the second subunit of the *E. coli* IDH. The identical residues between the monomeric and dimeric IDHs are colored in red, and the substrate and metal ion binding residues are boxed in yellow. Although Arg547 of the monomeric IDH and Arg153 of the dimeric IDH boxed in magenta are structurally identical for substrate binding, they cannot be aligned on this sequence alignment. The coenzyme binding residues of the dimeric IDH and those predicted for the monomeric IDHs are boxed in blue. No residue is found in the monomeric IDH, which corresponds to Arg395 of the dimeric IDH.

(B) The structure-based self-sequence alignment between two Greek key motifs in domain II of the *A. vinelandii* IDH. Some identical residues provide evidence of the partial gene duplication, so that these two IDHs are evolutionarily related.

Mn^{2+} is coordinated by O2 and O7 of isocitrate, Asp350 and Asp548 of the monomeric IDH, and two water molecules in an octahedral manner. The residues of Asp350 and Asp548 correspond to Asp283′ and Asp307 of the *E. coli* IDH, respectively. Thus, the amino acid residues of the monomeric IDH that bind to substrate and metal cation are completely identical to those of the dimeric IDH (Figures 4A and 6). Like the conservation of the critical residues, the structure of the catalytic site at the domain interface is also well superimposed, and the reaction mechanisms of both IDHs are considered to be identical.

Although the substrate and metal cation binding residues of both IDHs are identical, not all of these residues are conserved in the polypeptide chain shown in Figure 4A. Arg547 of the monomeric IDH and Arg153 of the dimeric IDH play an identical role in the structure by forming hydrogen bonds to O2 and O5 of isocitrate. These two arginine residues are located at completely different positions in the amino acid sequences. The 306th residue of the dimeric IDH, which is aligned with Arg547 of the monomeric IDH, is not arginine, but glycine, and the 411th residue of the monomeric IDH, which is aligned with Arg153 of the dimeric IDH, is also glycine, as shown in Figure 4A. These two arginine residues in the respective amino acid sequences are thus unrelated to each other.

Two identical subunits of the dimeric *E. coli* IDH are related by a crystallographic 2-fold axis, and, consequently, two catalytic sites are present per homodimeric form. On the other hand, the second catalytic site is absent in the structure of the monomeric IDH because of the lack of the domain corresponding to domain A of the second subunit of the dimeric IDH shown in Figure 5. Among the catalytic residues (corresponding to the

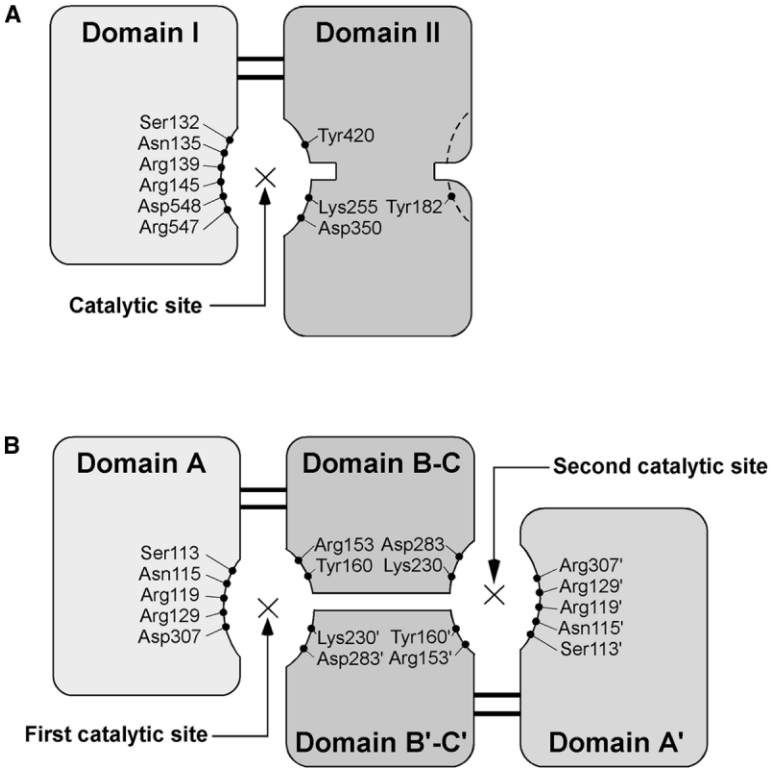

Figure 5. Schematic Representations of the Monomeric and Dimeric IDHs Showing the Distribution of Substrate and Metal Ion Binding Residues

(A) The *A. vinelandii* monomeric IDH. The structure of the monomeric IDH is formed by fusing domain B′-C′ of the dimeric IDH, so that the pseudo-2-fold axis exists in domain II. Arg547, which functionally corresponds to Arg153 of the dimeric IDH, belongs to domain I. Only one catalytic site is present per monomeric IDH molecule. Among the catalytic residues that existed in the primordial IDH (corresponding to the catalytic residues at the second catalytic site in the dimeric IDH [Lys230, Asp283, Arg153′, and Tyr160′]), only the tyrosine residue (Tyr182, corresponding to Try160′) is conserved.

(B) The *E. coli* dimeric IDH. Two identical subunits related by a 2-fold axis create two identical catalytic sites. Arg153, which functionally corresponds to Arg547 of the monomeric IDH, belongs to domain B.

second catalytic site in the dimeric IDH [Lys230, Asp283, Arg153′, and Tyr160′]), only the tyrosine residue of *A. vinelandii* and *C. maris* IDH (Tyr182, corresponding to Try160′) is conserved (Figure 4A).

Previous biochemical studies have attempted to determine the catalytic residues of the monomeric IDH. Met258 was proposed as one of the catalytic residues by the chemical modification with iodoacetic acid [4]. Although the structure of the monomeric IDH shows that Met258 interacts directly with neither isocitrate nor Mn^{2+}, it is located near the catalytic site (within 3.5 Å from isocitrate), and the carboxymethylation of this residue may lead to destruction of the catalytic site and inactivation of the enzyme. The activity of *A. vinelandii* IDH is also inhibited by treatment with modification reagents for the SH group, such as PCMB [12]. The structure of the monomeric IDH shows that all three of the free cysteine residues are located at the domain interface of domain II, near the active site. In particular, Cys459 is very close to the main chain of Tyr420, which binds directly to isocitrate, and the modification of this cysteine residue by PCMB treatment may prevent Tyr420 from binding to the substrate.

Prediction of the $NADP^+$ Binding Residues

The homodimeric IDH and IPMDH share a common protein folding and are unique in their lack of a common nucleotide binding motif, known as Rossmann fold [21]. The structure of the *E. coli* IDH complexed with $NADP^+$ has already been determined, and it revealed that the coenzyme binding pocket is constructed from two loops (βD–αJ and αh–βh) and one α helix (αL) [22, 23]. The present study revealed that the folding of the *A. vinelandii* IDH is homologous to that of the *E. coli* IDH and that it also lacks a Rossmann fold. Chen and Jeong suggested that coenzyme specificity in the *E. coli* dimeric IDH was conferred by the interactions between the side chains of Arg292′, Tyr345, Tyr391, Arg395 (by hydrogen bond), Lys344 (by ion pair), and the 2′-phosphate of $NADP^+$ [24]. On the basis of the structure-based sequence alignment shown in Figure 4A, Lys344, Tyr345, Arg292′, and Tyr391 of the *E. coli* IDH correspond to Lys588, His589, Arg358, and Arg649 of the monomeric IDH, respectively. These residues are located within a sphere with a radius of 10 Å. In contrast to the conservation of substrate and metal ion binding residues, these putative coenzyme binding residues are not completely identical to those of the *E. coli* IDH. Moreover, no residue corresponding to Arg395, which is located at a short helix (αL) of the *E. coli* IDH, is found either sequentially or structurally, as shown in Figures 2 and 4A. This helix (αL) is spatially conserved in both the holo form (Protein Data Bank ID 1AI2) [22] and apo form (Protein Data Bank ID 5ICD) [20] in the *E. coli* IDH. Thus, the interaction of the monomeric IDH with $NADP^+$ may be somewhat different from the dimeric IDH.

Evolution of the Monomeric IDH

Although the homology of the amino acid sequences between the monomeric and dimeric IDHs is no more than 7%–8%, which is much less than that between eukaryotic NAD^+-IDH and prokaryotic $NADP^+$-IDH (<17%) [23], the overall folding topology, as well as the conformation of the active site, is considerably con-

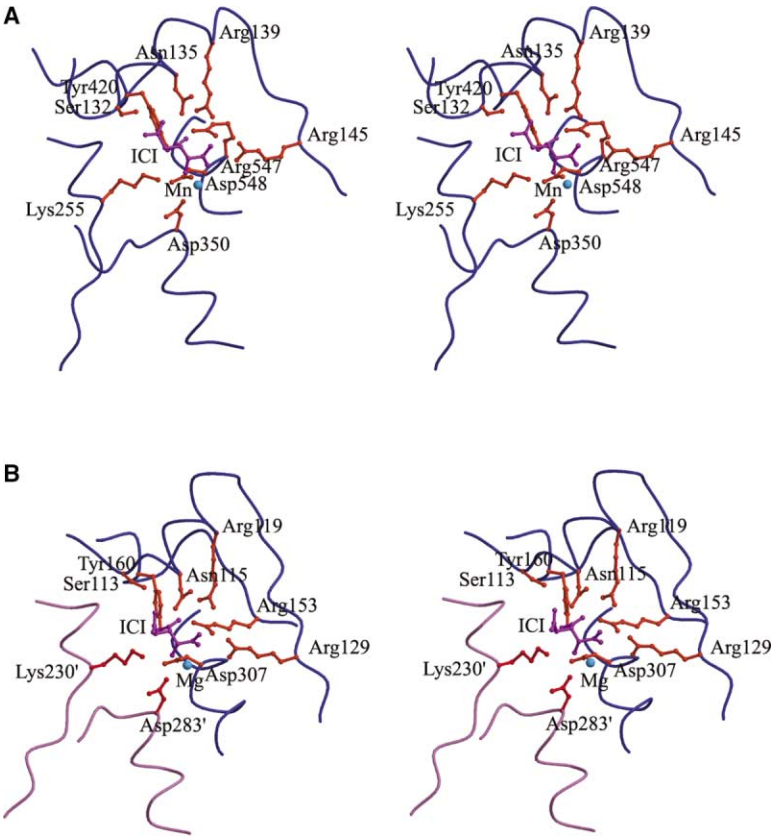

Figure 6. Structural Comparison between Substrate and Metal Ion Binding Sites of the Monomeric and Dimeric IDHs

(A) Stereo view of the substrate and metal ion binding site of the monomeric IDH from *A. vinelandii*. The isocitrate and Mn^{2+} binding residues of the monomeric IDH, red; the isocitrate molecule, magenta; Mn^{2+}, blue.

(B) Stereo view of the substrate and metal ion binding site of the dimeric IDH from *E. coli*. The isocitrate and Mg^{2+} binding residues of the dimeric IDH, red; the isocitrate molecule, magenta; Mg^{2+}, blue. Two residues (Lys230′ and Asp283′) belong to another subunit. The residues that construct the substrate and metal ion binding sites are completely identical between the monomeric and dimeric IDHs.

served. Furthermore, the sequence of the monomeric IDH can be very well aligned against most of the marker sequences of the β-decarboxylating dehydrogenase family shown in Figure 4A, and, thus, we concluded that these two IDHs are evolutionally related. A question then arises as to whether the present monomeic IDH has evolved from the dimeric IDH or independently from the primordial (hypothetical) monomeric IDH.

Several lines of evidence suggest that the monomeric IDH has evolved from the dimeric IDH. First, the folding of domain II seems to be created by repeating the same structural motif of domains B and C of the dimeric IDH. A structure-based self-sequence alignment in domain II of the monomeric IDH (Figure 4B) shows that, although the similarity is not high, several residues can be aligned between two Greek key motifs (β14–β17 and β18–β21), indicating that the monomeric IDH originated from partial gene duplication. Second, the atomic interactions around the pseudo-2-fold axis of domain II of the monomeric IDH are very similar to those of the interface between subunits of the dimeric IDH, suggesting that domains B and C were duplicated after the dimeric IDH created intensive interactions at the expansive intersubunit interface. Third, the monomeric IDH has most of the important structural framework of the dimeric IDH, e.g., the open twisted β sheet motif that spans both small and large domains.

Precise duplication of the domain B-C unit generates a domain-duplicated protein. Such a partial duplication of a domain unit is reminiscent of the exon shuffling (corresponding to the domain shuffling of the protein) in eukaryotes. The domain-shuffled proteins, such as certain transmembrane proteins in eukaryotes, acquire an entirely new function, since each domain usually has a specific and independent function. In contrast, the monomeric IDH is unique in that it has a function completely identical to that of other IDHs, and this domain duplication gives rise not to acquisition of a new function, but rather to monomerization of the IDH molecule that mimics the structure at the catalytic site. This evolutional pathway, from dimers to monomers, makes a sharp contrast with the evolutional process, from monomers to oligomers, by 3D domain swapping [24, 25].

Many examples of monomeric protein structures containing pseudo-2-fold symmetry exist [26]. Some of them, such as histidine biosynthetic enzyme homologs (HisF and HisA) and βB2-crystallin, are considered to have arisen from the gene duplication and fusion of the putative ancestral homodimers [27, 28]. Additionally, two examples of monomeric structures that partially mimic dimers by preserving the dimer interfaces essential for their functions are reported. The monomeric, allosterically regulated class II ribonucleotide reductase (RNR) retains the dimer interface responsible for effector binding in class I RNR, by fusing a small structural motif consisting of 130 residues [29]. The interdomain interface (tRNA binding site) in human monomeric endothelial monocyte-activating polypeptide II (EMAPII) mimics the intersubunit interface in bacterial dimeric tRNA binding proteins [30]. Like the monomeric IDH, both class II RNR and EMAPII might have arisen from the partial gene duplication of the corresponding ancestral gene, though

the sequence homologies between the putative duplicated regions of these proteins are very low. In the case of the monomeric IDH, the repetitive fold occurs on a larger scale than in class II RNR or EMAPII, and several residues can be aligned between two Greek key motifs (Figure 4B). Thus, the evolutional pathway of the monomeric IDH is more apparent than others.

It has been suggested that all IDHs (except the monomeric IDH) and IPMDH evolved from a common ancestral protein having broad substrate specificity with the 2-*R* malate carbon skeleton, $^{-}OOC(HO)CHCH(X)COO^{-}$ [31]. On the basis of the present study of the monomeric IDH, we suggest that the monomeric IDH was separated from an ancestral protein that was specific for isocitrate. The substrate binding residues are absolutely identical between the monomeric and dimeric IDHs, and these equivalent residues would suggest that the acquisition of the substrate specificity might have occurred once for all IDHs through an evolutional process. In other words, the ancestral gene was duplicated after this ancestral protein acquired the isocitrate specificity, and each gene would have evolved independently. This hypothesis also explains the existence of bacteria, such as *C. maris* and *P. aeruginosa*, that possess both monomeric and dimeric IDHs ([5, 32] and searches by database). According to this scenario, Arg547 would have taken over the role of Arg153 after incidental mutations.

Monomeric IDHs and the putative monomeric IDH genes have been found only in prokaryotes. It is noteworthy that the 16S rRNA gene analysis revealed no phylogenetic relationships among these prokaryotes (data not shown) and that these bacteria contain both gram-positive and -negative species. Thus, the monomeric IDH first appeared in the period between the branch point of prokaryote/eukaryote (between 2 and 3.5 billion years ago) and that of gram-positive/negative bacteria (1 billion years ago). The prokaryotes that possess only the monomeric IDH at present might have possessed both monomeric and dimeric IDHs in that time period, as in the case of *C. maris* and *P. aeruginosa*. They would then have chosen either one of the IDHs in the course of eubacterial diversification. This hypothesis would explain why these taxonomically unrelated prokaryotes possess the monomeric IDH at present. Certainly these prokaryotes have their own rationales for preserving the monomeric IDH for metabolism, such as for cold adaptation in the case of *C. maris*.

Biological Implications

All prokaryotic IDHs are either dimeric or monomeric enzymes and catalyze the oxidative decarboxylation step from 2*R*,3*S*-isocitrate to 2-oxoglutarate, using $NADP^{+}$ as a cofactor [1]. This reaction is the rate-limiting step in the Krebs cycle, so that the IDH is the key regulated enzyme of the cycle. The dimeric IDH is distributed ubiquitously in a wide variety of prokaryotes, while the monomeric IDH is present only in a few taxonomically unrelated eubacteria. The structure of the dimeric *E. coli* IDH has previously been determined. The active site of the dimeric IDH was located at the intersubunit interface and was formed by the residues from both subunits [20, 23]. In contrast, the monomeric IDH apparently catalyzes a reaction identical to that of the dimeric IDH with a single polypeptide chain.

Here we describe, for the first time, the crystal structure of the monomeric IDH, complexed with substrate and Mn^{2+}. The overall structure of the monomeric IDH shows that a single polypeptide chain ingeniously folds by fusing the partial domain structure of the dimeric IDH, and the conformation of the active site admirably mimics that of the dimeric IDH. The present study also reveals that both IDHs predominantly share a common folding topology. The structure-based sequence alignment between these two IDHs suggests that the monomeric IDH originated from partial gene duplication, and, thus, we concluded that the monomeric IDH divergently evolved from the dimeric IDH. This evolutional pathway, from dimers to monomers, makes a sharp contrast with the molecular evolution toward oligomerization by 3D domain swapping.

Experimental Procedures

Protein Purification and Crystallization

The monomeric isocitrate dehydrogenase was purified from nitrogen-fixing bacterium *Azotobacter vinelandii* (IAM1078) cells. The crystals of the orthorhombic form were grown under the condition of 0.1 M HEPES-NaOH (pH 7.0), 24%–28% (w/v) polyethylene glycol 6000, 20.0% (v/v) glycerol, 4.0 mM isocitrate, and 4.0 mM $MnCl_2$. The details of the protein purification and the crystallization procedure were described previously [16]. During the MAD phase calculation, the crystal of monoclinic form, which was used for collecting a higher-resolution data set, was obtained under the same condition.

Data Collection and Processing Procedure

The crystals of each form were grown in a solution containing 20% (v/v) glycerol, so that they could be flash-cooled without soaking in a cryoprotectant. However, the flash-cooled crystals prepared with CryoLoop (Hampton Research) diffracted with extremely high mosaicity. We therefore attempted to flash cool the crystals in a capillary and succeeded in collecting good diffraction data with low mosaicity.

A Mn MAD data set was collected to 2.9 Å resolution from one crystal of the orthorhombic form on beamline BL41XU at SPring-8, Japan. The crystal belongs to space group $P2_12_12_1$, with unit cell dimensions of a = 108.4 Å, b = 121.7 Å, and c = 129.7 Å, and there are two molecules in the asymmetric unit. Three wavelengths were selected on the basis of the fluorescence spectrum of the Mn K edge, corresponding to the maximum f″ (peak, 1.8923 Å), the minimum f′ (edge, 1.8934 Å), and a reference point (remote, 1.8783 Å). The diffraction spots were indexed and integrated with the program MOSFLM [33]. The diffraction intensities were scaled to a reference data set that was calculated from all three data sets with the program SCALA (relative scaling) [34]. This relative scaling procedure also included smooth scaling across the detector (three-dimensional scaling), which partly corrected the systematic errors caused by the absorption effect [16]. A higher-resolution data set was collected from the monoclinic crystal on beamline BL41XU at SPring-8, Japan. The crystal belongs to space group $P2_1$, with unit cell dimensions of a = 110.4 Å, b = 119.0 Å, c = 128.2 Å, and $\beta = 99.0^{\circ}$, and there are four molecules in the asymmetric unit. The diffraction data were indexed and integrated to a resolution of 1.95 Å with the program MOSFLM [33] and scaled with the program SCALA [34]. The data collection and processing statistics are shown in Table 1.

Structure Determination and Refinement

The heavy-atom parameters refinement and the MAD phase calculation were achieved with the program SHARP [35], with only two Mn atoms in an asymmetric unit, which bound to two independent monomeric IDH molecules. The translational operator of the noncrystallographic symmetry (NCS) was determined with the program AMoRe [36] and improved by IMP of the Uppsala program package

Table 1. Data Collection and Refinement Statistics

Data Collection Statistics	
Beamline	BL41XU, SPring-8
Space group	$P2_1$
Cell dimensions	a = 110.4 Å b = 119.0 Å c = 128.2 Å β = 99.0°
Wavelength (Å)	0.9000
Resolution range (Å)[a]	40–1.95 (2.06–1.95)
Number of observed reflections	846,014
Number of unique reflections	235,314
Completeness (%)[a]	98.9 (96.7)
Multiplicity[a]	3.6 (3.2)
Averaged I/σ (I)[a]	8.6 (2.0)
R_{meas}[a,b]	0.083 (0.388)
Refinement Statistics	
Resolution range (Å)	10–1.95
Number of reflections	233,612
R factor[c]	0.193
R_{free} factor[d]	0.228
Number of residues	2,959
Number of nonhydrogen atoms	24,950
Number of water molecules	2,306
Average B factor (Å^2)	23.51
Rmsd bond lengths (Å)	0.0049
Rmsd bond angles (°)	1.23
Ramachandran plot	
Residues in most-favored regions (%)	91.2
Residues in additional allowed regions (%)	8.5
Residues in generously allowed regions (%)	0.3

[a] The values in parentheses refer to data in the highest resolution shell (2.06–1.95 Å).
[b] $R_{meas} = \Sigma_h[m/(m-1)]^{1/2}\Sigma_i|I_{h,i} - \langle I_h\rangle|/\Sigma_h\Sigma_i|I_{h,i}|$, where $\langle I_h\rangle$ is the mean intensity of a set of equivalent reflections and m is the multiplicity of the data set.
[c] R factor $= \Sigma|F_{obs} - F_{calc}|/\Sigma F_{obs}$, where F_{obs} and F_{calc} are the observed and calculated structure factor amplitudes.
[d] R_{free} factor was calculated for R factor, using a random 10% subset from all reflections.

[37] after map improvement by solvent flattening with the program SOLOMON [38] by the procedure in the program SHARP. Although some secondary structures were recognized at this step, the initial electron density map was not good enough for building the whole model, and further phase improvement by NCS averaging was not effective because of the translational NCS [37]. After some polyalanine fragments were built on the graphic program O [39] with the poor-quality experimental map calculated with density modification with the program DM [40], phase improvement was carried out by the procedure of the properly weighted phase combination with the program SIGMAA [41]. In this procedure, three phase sets, (1) calculated after SHARP [35], (2) calculated after DM [40], and (3) calculated from the partial structures of polyalanine fragments, were combined, and a partial polyalanine model consisting of 591 out of 741 residues (almost 80% of the overall structure) was successfully built.

For obtaining the whole structure of the monomeric IDH, a higher-resolution data set of the monoclinic form was indispensable. The molecular replacement with the program AMoRe [36] was carried out with the partial structures of the polyalanine model as a search model, and the four relationships of the IDH molecules between $P2_12_12_1$ and $P2_1$ cells were determined, corresponding to four independent IDH molecules in an asymmetric unit of $P2_1$ form. The electron density map was dramatically improved by multicrystal averaging with the program DMMULTI [40], and the atomic model of the monomeric IDH, except for a few loop regions, was easily built into the experimental electron density map (15–2.9 Å). The MAD-phasing statistics are shown in Table 2. Further phase improvement and extension to a resolution of 1.95 Å were carried out on the monoclinic $P2_1$ form, with the program DM [40]. The improved map was of high quality, and the complete atomic model was rebuilt. The positional, simulated annealing and the temperature factor refinement were performed, and the water molecules were located automatically with the program CNS [42]. To monitor the refinement, we set aside 10% of the reflection data for the calculation of the free R factor. The final model consists of 2959 residues, 2306 water molecules, 4 isocitrate molecules, and 5 manganese ions (4 ions are found at the active site, and 1 is found at the surface of an IDH molecule), with an R factor of 19.3% and a free R factor of 22.8%. The stereochemical quality of this atomic model was checked with the program PROCHECK [43]. Refinement statistics are shown in Table 1.

Acknowledgments

We would like to thank Dr. Kawamoto of the Japan Synchrotron Radiation Research Institute (JASRI) for his kind help in Mn MAD data collection on beamline BL41XU at SPring-8, Japan. This work was supported in part by research grants from a Grant-in-Aid for Scientific Research and a National Project on Protein Structural and Functional Analyses from the Ministry of Education, Culture, Sports, Science and Technology of Japan.

Received: June 5, 2002
Revised: August 30, 2002
Accepted: September 10, 2002

Table 2. Phasing Statistics of Mn MAD Data (15–2.9 Å)

		Remote		Peak		Edge	
		Isomorphous	Anomalous	Isomorphous	Anomalous	Isomorphous	Anomalous
R_{cullis}[a]	Centric	—	—	0.532	—	0.526	—
	Acentric	—	0.871	0.493	0.802	0.494	0.882
R_{kraut}[b]	Centric	0.304	0.537	0.252	0.465	0.240	0.483
	Acentric	0.030	0.053	0.025	0.046	0.024	0.048
Phasing power[c]	Centric	—	—	1.04	—	1.20	—
	Acentric	—	1.20	1.43	1.64	1.68	1.13
FOM	Centric	0.18					
	Acentric	0.33					
FOM after DMMULTI[d]		0.74					

[a] $R_{cullis} = \langle$phase-integrated lack of closure$\rangle/\langle|F_{PH} - F_P|\rangle$.
[b] $R_{kraut} = \langle$phase-integrated lack of closure$\rangle/\langle|F_{PH}|\rangle$.
[c] Phasing power $= \langle|F_H(calc)|\rangle/\langle E\rangle$, where E is the phase-integrated lack of closure.
[d] Figure of merit after the multicrystal averaging with the program DMMULTI.

References

1. Chen, R.D., and Gadal, P. (1990). Structure, function and regulation of NAD and NADP dependent isocitrate dehydrogenase in higher plants and in other organisms. Plant Physiol. Biochem. *28*, 411–427.
2. Hurley, J.H., Thorsness, P.E., Ramalingam, V., Helmers, N.H., Koshland, D.E., Jr., and Stroud, R.M. (1989). Structure of a bacterial enzyme regulated by phosphorylation, isocitrate dehydrogenase. Proc. Natl. Acad. Sci. USA *86*, 8635–8639.
3. Imada, K., Sato, M., Tanaka, N., Katsube, Y., Matsuura, Y., and Oshima, T. (1991). Three-dimensional structure of a highly thermostable enzyme, 3-isopropylmalate dehydrogenase of *Thermus thermophilus* at 2.2 Å resolution. J. Mol. Biol. *222*, 725–738.
4. Chung, A.E., and Franzen, J.S. (1969). Oxidized triphosphopyridine nucleotide specific isocitrate dehydrogenase from *Azotobacter vinelandii*: isolation and characterization. Biochemistry *8*, 3175–3184.
5. Ochiai, T., Fukunaga, N., and Sasaki, S. (1979). Purification and some properties of two $NADP^+$-specific isocitrate dehydrogenases from an obligately psychrophilic marine bacterium, *Vibrio* sp., strain ABE-1. J. Biochem. (Tokyo) *86*, 377–384.
6. Eikmanns, B.J., Rittmann, D., and Sahm, H. (1995). Cloning, sequence analysis, expression, and inactivation of the *Corynebacterium glutamicum icd* gene encoding isocitrate dehydrogenase and biochemical characterization of the enzyme. J. Bacteriol. *177*, 774–782.
7. Leyland, M.L., and Kelly, D.J. (1991). Purification and characterization of a monomeric isocitrate dehydrogenase with dual coenzyme specificity from the photosynthetic bacterium *Rhodomicrobium vanniellii*. Eur. J. Biochem. *202*, 85–93.
8. Fukunaga, N., Imagawa, S., Sahara, T., Ishii, A., and Suzuki, M. (1992). Purification and characterization of monomeric isocitrate dehydrogenase with $NADP^+$-specificity from *Vibrio parahaemolyticus* Y-4. J. Biochem. (Tokyo) *112*, 849–855.
9. Steen, I.H., Madsen, M.S., Birkeland, N.K., and Lien, T. (1998). Purification and characterization of a monomeric isocitrate dehydrogenase from the sulfate-reducing bacterium *Desulfobacter vibrioformis* and demonstration of the presence of a monomeric enzyme in other bacteria. FEMS Microbiol. Lett. *160*, 75–79.
10. Sahara, T., Takada, Y., Takeuchi, Y., Yamaoka, N., and Fukunaga, N. (2002). Cloning, sequencing, and expression of a gene encoding the monomeric isocitrate dehydrogenase of the nitrogen fixing bacterium, *Azotobacter vinelandii*. Biosci. Biotechnol. Biochem. *66*, 489–500.
11. Ishii, A., Suzuki, M., Sahara, T., Takada, Y., Sasaki, S., and Fukunaga, N. (1993). Genes encoding two isocitrate dehydrogenase isozymes of a psychrophilic bacterium, *Vibrio* sp. strain ABE-1. J. Bacteriol. *175*, 6873–6880.
12. Barrera, C.R., and Jurtshuk, P. (1970). Characterization of the highly active isocitrate ($NADP^+$) dehydrogenase of *Azotobacter vinelandii*. Biochim. Biophys. Acta *220*, 416–429.
13. Suzuki, M., Sahara, T., Tsuruha, J., Takada, Y., and Fukunaga, N. (1995). Differential expression in *Escherichia coli* of the *Vibrio* sp. strain ABE-1 *icdI* and *icdII* genes encoding structurally different isocitrate dehydrogenase isozymes. J. Bacteriol. *177*, 2138–2142.
14. Chen, R., and Yang, H. (2000). A highly specific monomeric isocitrate dehydrogenase from *Corynebacterium glutamicum*. Arch. Biochem. Biophys. *383*, 238–245.
15. Czerwizski, E.W., Bethge, P.H., Mathews, F.S., and Chung, A.E. (1977). A preliminary crystallographic study of isocitrate dehydrogenase from *Azotobacter vinelandii*. J. Mol. Biol. *116*, 181–187.
16. Yasutake, Y., Watanabe, S., Yao, M., Takada, Y., Fukunaga, N., and Tanaka, I. (2001). Crystallization and preliminary X-ray diffraction studies of monomeric isocitrate dehydrogenase by the MAD method using Mn atoms. Acta Crystallogr. D *57*, 1682–1685.
17. Holm, L., and Sander, C. (1993). Protein structure comparison by alignment of distance matrices. J. Mol. Biol. *233*, 123–138.
18. Hurley, J.H., Chen, R., and Dean, A.M. (1996). Determinants of cofactor specificity in isocitrate dehydrogenase: structure of an engineered $NADP^+ \rightarrow NAD^+$ specificity-reversal mutant. Biochemistry *35*, 5670–5678.
19. Wallon, G., Kryger, G., Lovett, S.T., Oshima, T., Ringe, D., and Petsko, G.A. (1997). Crystal structures of *Escherichia coli* and *Salmonella typhimurium* 3-isopropylmalate dehydrogenase and comparison with their thermophilic counterpart from *Thermus thermophilus*. J. Mol. Biol. *266*, 1016–1031.
20. Hurley, J.H., Dean, A.M., Sohl, J.L., Koshland, D.E., Jr., and Stroud, R.M. (1990). Regulation of an enzyme by phosphorylation at the active site. Science *249*, 1012–1016.
21. Rossmann, M.G., Moras, D., and Olsen, K.W. (1974). Chemical and biological evolution of a nucleotide-binding protein. Nature *250*, 194–199.
22. Hurley, J.H., Dean, A.M., Koshland, D.E., Jr., and Stroud, R.M. (1991). Catalytic mechanism of $NADP^+$-dependent isocitrate dehydrogenase: implications from the structures of magnesium-isocitrate and $NADP^+$ complexes. Biochemistry *30*, 8671–8678.
23. Chen, R., and Jeong, S.S. (2000). Functional prediction: identification of protein orthologs and paralogs. Protein Sci. *9*, 2344–2353.
24. Bennett, M.J., Schlunegger, M.P., and Eisenberg, D. (1995). 3D domain swapping: a mechanism for oligomer assembly. Protein Sci. *12*, 2455–2468.
25. Schlunegger, M.P., Bennett, M.J., and Eisenberg, D. (1997). Oligomer formation by 3D domain swapping: a model for protein assembly and misassembly. Adv. Protein Chem. *50*, 61–122.
26. Kinch, L.N., and Grishin, N.V. (2002). Evolution of protein structure and functions. Curr. Opin. Struct. Biol. *12*, 400–408.
27. Hocker, B., Beismann-Driemeyer, S., Hettwer, S., Lustig, A., and Sterner, R. (2001). Dissection of a $(\beta\alpha)_8$-barrel enzyme into two folded halves. Nat. Struct. Biol. *8*, 32–36.
28. Clout, N.J., Basak, A., Wieligmann, K., Bateman, O.A., Jaenicke, R., and Slingsby, C. (2000). The N-terminal domain of βB2-crystallin resembles the putative ancestral homodimer. J. Mol. Biol. *304*, 253–257.
29. Sintchak, M.D., Arjara, G., Kellogg, B.A., Stubbe, J., and Drennan, C.L. (2002). The crystal structure of class II ribonucleotide reductase reveals how an allosterically regulated monomer mimics dimer. Nat. Struct. Biol. *9*, 293–300.
30. Renault, L., Kerjan, P., Pasqualato, S., Menetrey, J., Robinson, J.-C., Kawaguchi, S., Vassylyev, D.G., Yokoyama, S., Mirande, M., and Cherfils, J. (2001). Structure of the EMAPII domain of human aminoacyl-tRNA synthetase complex reveals evolutionary dimer mimicry. EMBO J. *20*, 570–578.
31. Dean, A.M., and Golding, G.B. (1997). Protein engineering reveals ancient adaptive replacements in isocitrate dehydrogenase. Proc. Natl. Acad. Sci. USA *94*, 3104–3109.
32. Ishii, A., Ochiai, T., Imagawa, S., Fukunaga, N., Sasaki, S., Minowa, O., Mizuno, Y., and Shiokawa, H. (1987). Isozymes of isocitrate dehydrogenase from an obligatory psychrophilic bacterium, *Vibrio* sp. strain ABE-1: purification, and modulation of activities by growth conditions. J. Biochem. (Tokyo) *102*, 1489–1498.
33. Leslie, A.G.W. (1993). Auto-indexing of rotation diffraction images and parameter refinement. In Proceedings of the CCP4 Study Weekend, L. Sawyer, N. Isaacs, and S. Bailey, eds. (Daresbury, UK: Daresbury Laboratory), pp. 44–51.
34. CCP4 (Collaborative Computational Project 4). (1994). The CCP4 suite: programs for protein crystallography. Acta Crystallogr. D Biol. Crystallogr. *50*, 760–763.
35. de La Fortelle, E., and Bricogne, G. (1997). Maximum-likelihood heavy-atom parameter refinement for multiple isomorphous replacement and multiwavelength anomalous diffraction methods. Methods Enzymol. *276*, 472–494.
36. Navaza, J. (1994). AmoRe: an automated package for molecular replacement. Acta Crystallogr. A *50*, 157–163.
37. Kleywegt, G.J., and Read, R.J. (1997). Not your average density. Structure *5*, 1557–1569.
38. Abrahams, J.P., and Leslie, A.G.W. (1996). Methods used in the structure determination bovine mitochondrial F1 ATPase. Acta Crystallogr. D *52*, 30–42.
39. Jones, T.A., Zou, J.Y., Cowan, S.W., and Kjeldgaard, M. (1991). Improved methods for building protein models in electron den-

sity maps and the location of errors in these methods. Acta Crystallogr. A *47*, 110–119.
40. Cowtan, K. (1994). dm: an automated procedure for phase improvement by density modification. Joint CCP4 and ESF-EACBM Newsletter on Protein Crystallography *31*, 34–38.
41. Read, R.J. (1986). Improved Fourier coefficients for maps using phases from partial structures with errors. Acta Crystallogr. A *42*, 140–149.
42. Brunger, A.T., Adams, P.D., Clore, G.M., DeLano, W.L., Gros, P., Grosse-Kunstleve, R.W., Jiang, J.-S., Kuszewski, J., Nilges, M., Pannu, N.S., et al. (1998). Crystallography and NMR system (CNS): a new software system for macromolecular structure determination. Acta Crystallogr. D *54*, 905–921.
43. Laskowski, R.A., Mac Arthur, M.W., Moss, D.S., and Thornton, J.M. (1993). PROCHECK: a program to check the stereochemical quality of protein structures. J. Appl. Crystallogr. *26*, 283–291.

Accession Numbers

The atomic coordinates of the monomeric IDH in complex with isocitrate and Mn^{2+} have been deposited in the Protein Data Bank under accession code 1ITW.